TNO (278361) 2007 JJ 43 observed with X-Shooter

F. Gourgeot, M. Barucci, A. Alvarez-Candal, F. Merlin, D. Perna, D. Lazzaro

A&A 582, A13 (2015)
DOI: 10.1051/0004-6361/201526014

Astronomy & Astrophysics

TNO (278361) 2007 JJ_{43} observed with X-Shooter *(Research Note)*

F. Gourgeot[1,2], M. A. Barucci[2], A. Alvarez-Candal[1], F. Merlin[2,3], D. Perna[2], and D. Lazzaro[1]

[1] Observatorio Nacional, COAA, Rua General Jose Cristino 77, 20921-400 Rio de Janeiro, Brazil
e-mail: gourgeot@on.br
[2] Observatoire de Paris-Meudon / LESIA, Meudon, 75014 Paris, France
[3] Université Denis Diderot, Paris VII, 75013 Paris, France

Received 3 March 2015 / Accepted 28 June 2015

ABSTRACT

Context. The trans-Neptunian region of the solar system is populated by a wide variety of icy bodies showing great diversity in orbital behavior, size, surface color, and composition.
Aims. We present new ultraviolet, visible and near-infrared spectroscopic measurements for the trans-Neptunian object (278361) 2007 JJ_{43}, which is a dwarf planet candidate.
Methods. The observations were performed with the instrument X-Shooter for the 8.2 m ESO Very Large Telescope mounted on the UT2 at the Paranal Observatory in Chile. This spectrograph covers the entire 300–2480 nm spectral range at once with a high resolving power. We analyzed the surface composition by modeling the spectra in the complete wavelength range and tried to detect icy compounds. We searched for spectral heterogeneity by comparing spectra obtained at different regions.
Results. The spectrum obtained is quite flat and 2007 JJ_{43} can be classified as a blue-red object. No absorption bands of icy elements were detected in the spectra. However, our models indicate that crystalline water ice is probably not present on the surface in more than a concentration of 6.5%. Observations covering about one-third of the entire surface do not present any differences, suggesting that the surface is apparently homogeneous.

Key words. Kuiper belt objects: individual: (278361) 2007 JJ_{43} – techniques: spectroscopic – instrumentation: spectrographs

1. Introduction

The trans-Neptunian objects (TNO) are located in the Edgeworth-Kuiper Belt beyond the orbit of Neptune. At present, almost 1400 objects have been discovered and are listed in the Minor Planet Center (MPC) database. In this paper, we present observations of (278361) 2007 JJ_{43}, one of the largest TNO, which was discovered by Schwamb et al. (2007) at the Palomar Observatory. Dynamically it is classified as a classical object (Cubewano) presenting the following orbital parameters (Schwamb et al. 2007): a semi-major axis of 47.8 AU, an eccentricity of 0.16, an inclination of 12.06, and a revolution period of about 330.74 years. Its rotational period has recently been determined by Benecchi & Sheppard (2013) to be 6.04 h. Using the measured absolute magnitude, between 3.2 and 3.9 (Sheppard et al. 2011; Benecchi & Sheppard 2013), its diameter has been estimated to be between 650 and 800 km, similar to that of the TNO (28978) Ixion which is a good candidate to be a dwarf planet. It is noteworthy that TNO surfaces are among the most pristine material in the solar system and the spectra of some of these objects present signature of various ices (such as water, methane, methanol and nitrogen). In this sense, (278361) 2007 JJ_{43} is an interesting object to study and the use of the VLT with the X-Shooter instrument can characterize its surface composition to verify whether there are any icy components.

2. Observations and data reduction

2.1. X-Shooter

X-Shooter is the first of the second-generation instruments at the VLT. This instrument is an echelle spectrograph that has an almost fixed spectral setup. A detailed description of the instrument is available at ESO's webpage[1]. This spectrograph has the ability to simultaneously obtain data over the entire 300–2480 nm spectral range by splitting the incoming light from the telescope into three beams, each sent to a different arm: ultraviolet-blue (UVB), visible (VIS), and near-infrared (NIR). Using two dichroics, the light is first sent to the UVB arm, then to the VIS arm, and the remaining light reaches the NIR arm. The disadvantage of this optical path is the high thermal background in the K region of the NIR spectrum. Each arm operates independently of the others, with the sole exception of the UVB and VIS CCD, which share the same controller and cannot be read simultaneously. The read-out of the NIR detector is totally independent of the others, operated by an Infra Red Array Control Electronics (IRACE) controller.

2.2. Observations

2007 JJ_{43} was observed on 2009 May 8th during the verification and calibration phases of the X-Shooter instrument (Prog ESO ID: 60.A-9024-A). Four observations of half an hour each (total of 2h) were performed (see Table 1). One solar analog was observed: HIP 79658 (G1V type). We used the SLIT mode, selecting the high-gain readout mode and 2×1 binning for the UVB and VIS detectors. We nodded on the slit to remove the sky contribution, as usual for NIR observations. The read-out and binning for the NIR detector are fixed. The slit widths were

[1] http://www.eso.org/sci/facilities/paranal/instruments/xshooter

Table 1. Observation table of 2007 JJ_{43} and of the used analog star.

Object (notation)	Date	Time (hh:mm:ss)*	Airmass**	Seeing(″)**	Exp. time (s)
2007 JJ_{43}_1	2009-05-08	07:02:27	1.082–1.145	1.26–1.19	1800
2007 JJ_{43}_2	2009-05-08	07:34:08	1.149–1.240	1.10–1.19	1800
2007 JJ_{43}_3	2009-05-08	08:05:36	1.244–1.372	1.30–1.00	1800
2007 JJ_{43}_4	2009-05-08	08:37:15	1.378–1.561	0.90–1.01	1800
HIP 79658(type G1V)	2009-05-08	09:16:07	1.247–1.249	1.08–1.08	2
HIP 79658(type G1V)	2009-05-08	09:17:47	1.253–1.255	1.32–1.32	2

Notes. (*) Time UT corresponding to the beginning of the observations. (**) Values of airmass and seeing are from the beginning to the end of each observation.

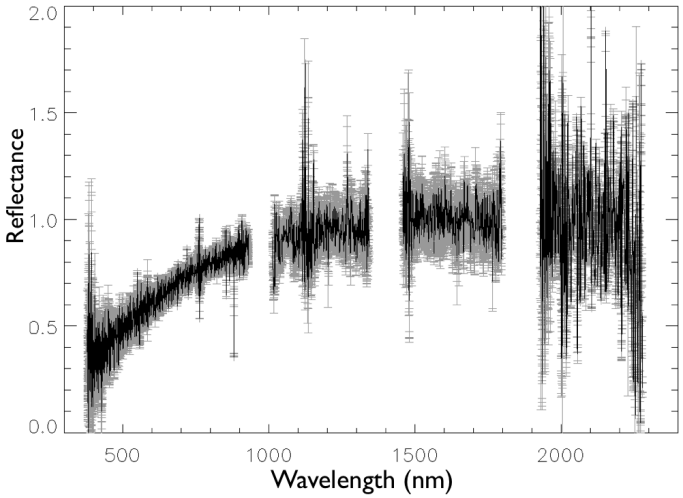

Fig. 1. Final spectrum of 2007 JJ_{43} combining the spectra in UVB, VIS and NIR obtained by the three arms of the X-Shooter instrument. Error bars correspond to the standard deviation of one sigma while the gaps depict the telluric atmosphere absorption. The spectrum has been normalized to unity at 1.75 μm, by convention.

1.0″, 0.9″, and 0.9″, for the UVB, VIS, and NIR arms, respectively, yielding a resolving power of about 5000 per arm.

2.3. Data reduction

The data were reduced using the X-Shooter pipeline (2.0.0): wavelength calibration is performed by using a two-dimensional wave-map. This is necessary because of the curvature of the echelle orders. The map was created by taking images of thorium and argon lamps combined with pinhole masks for all three arms. The final accuracy of the calibration is better than 0.1 nm throughout the complete spectral range. Although the pipeline extracts the 1D spectrum from a 2D image, we preferred instead to extract the 1D spectrum ourselves after verifying the best quality of our own extraction. The extraction was made in the usual way with the *apall* application from IRAF. Once all spectra were extracted, we divided those of 2007 JJ_{43} by that of the star HIP 79658, used as telluric and solar analog star (Table 1). After the division we removed the remaining bad pixels from the spectra using a median filtering technique (as in Alvarez-Candal et al. 2007). This last step resulted in three separated spectra, one per arm. However, since their spectral ranges overlap slightly, the construction of the final spectrum is straightforward. The resulting spectrum, spanning the complete range between 350 and 2350 nm is presented in Fig. 1. The spectrum was normalized to unity at 1750 nm by convention.

3. Results

The final spectrum (Fig. 1) corresponds to the average of the four individual spectra cleaned from bad pixels. The associated error represents the standard deviation measured at one σ. The obtained spectrum shows a relatively red behavior with no clear absorption band such as water ice, for instance. There is a strong increase of reflectance from 350 to 1500 nm. In the region from 1500 up to 1800 nm, the spectrum becomes flat and is followed by a decrease of the reflectance in the region from 1900 nm to 2300 nm. It is noteworthy that the very low signal-to-noise (S/N) in the NIR region is due to the high thermal background in this region, as mentioned before.

The possible heterogeneity of the surface was also studied by analyzing the individual spectra. To increase the S/N we combined the four spectra into two, representing the first and second half of the observation. The obtained spectra are JJ_{43}_12 and JJ_{43}_34, indicating the combination of the first with the second and the third with the fourth spectrum, respectively. These spectra are shown in Figs. 2 and 3 considering all the spectral range (ALL) and the three separate regions (UBV, VIS, NIR) corresponding to each X-Shooter arm. We also plotthe ratio between the spectra in each spectral region to better visualize distinct features.

No significant difference between the two spectra can be identified up to the S/N resolution of the observations. This is an indication that the two surface regions spanned by the observations could present a similar composition. As can be seen in Figs. 2 and 3, the ratio spectrum is flat in the visible and in the near-infrared ranges. The differences present in the ultraviolet region (between 350 and 450 nm) are linked to the low S/N. Indeed, the UVB spectra variation is connected to the lowest resolution of X-Shooter in this wavelength (the resolving power associated with the slit is about 4350 for UVB whereas it is up to 5300 for both other arms[2]), it is quite difficult to distinguish small spectral differences in this part. The differences observed in the 1100–1150 nm and 1950–2000 nm regions are artifacts introduced by the star and poor telluric correction, respectively. A small feature can be observed around 1500-1550 nm but the depth of the absorption band is smaller than the uncertainties and its position does not correspond to any known spectral band; possibly, this is an artifact.

We can thus conclude that no relevant spectral difference is detected between the beginning and the end of the observation. Since the rotational period is about six hours and our observations span a two-hour interval, then the observed region is nearly one-third of the entire surface (the sub-Earth longitude of the

[2] More information about the characteristics of each slit resolution is available at https://www.eso.org/sci/facilities/paranal/instruments/xshooter/inst.html

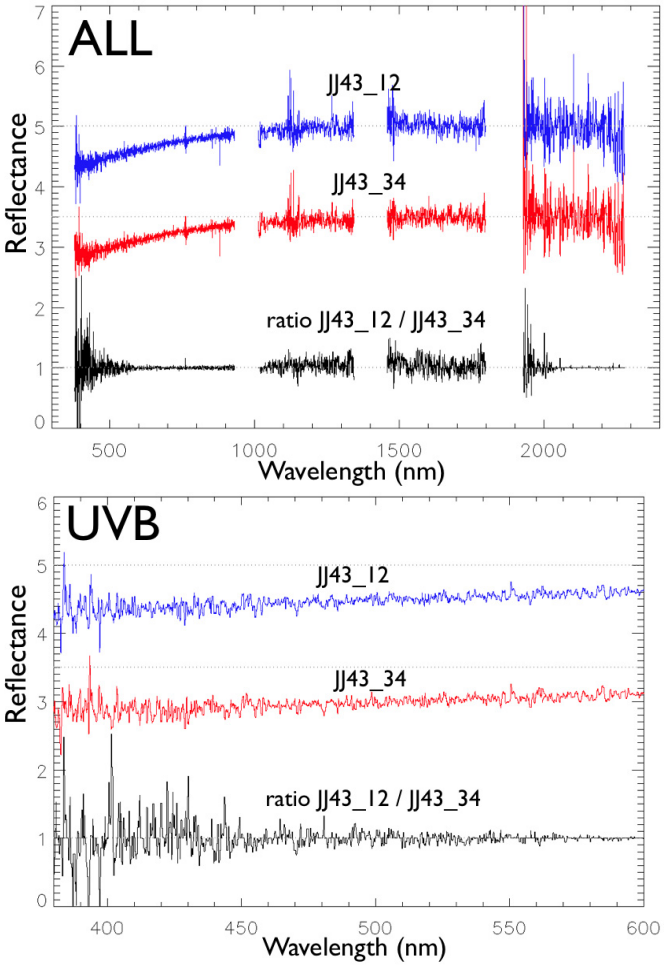

Fig. 2. Spectra corresponding to the first (blue) and the second (red) part of the observation along with the associated ratio between them (black). "All" stands for all the studied spectral domain and "UVB" for the ultraviolet-blue. The spectra have been normalized to unity at 1.75 μm and shifted for clarity by 2.5 and 3 units.

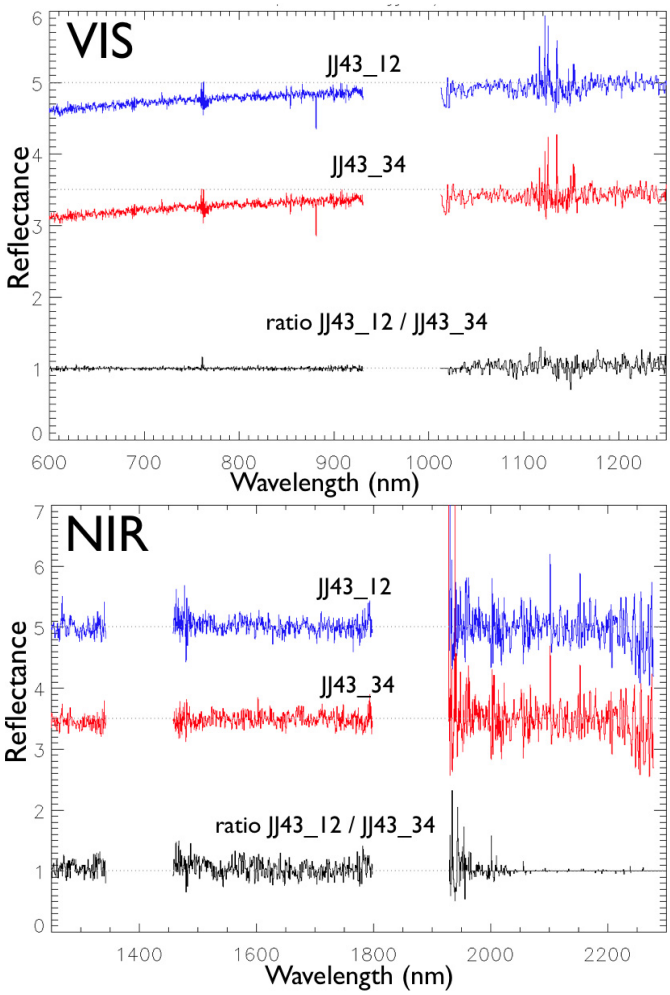

Fig. 3. Same as Fig. 1, where "VIS" stand for visible (*up*) and "NIR" for near-infrared (*bottom*). The spectra have been normalized to unity at 1.75 μm and shifted for clarity by 2.5 and 3 units.

center of the observed disk covers 120°). Therefore, we can argue that the surface of 2007 JJ_{43} is possibly homogenous.

Finally, we used the combined spectrum (Fig. 1) to classify 2007 JJ_{43} according to the TNO taxonomy derived from photometric colors (Barucci et al. 2005; Perna et al. 2010). The diverse classes separate the objects according to their slope going from the reddest (RR) to the bluest (BB) and with two intermediate classes: blue-red (BR) and intermediate red (IR). In Fig. 4 we plot the photometric values of the four classes along with the 2007 JJ_{43} spectrum. Computing the difference (χ^2) between our spectrum and the diverse classes, we obtain the values of 63.6, 5.0, 17.6 and 21.7 for the BB, BR, IR and RR classes, respectively. Considering the smallest χ^2, then 2007 JJ_{43} can be classified as a BR object.

4. Modeling

4.1. Methods

We used the spectral model developed by (Hapke 1981, 1993) to set the limits on the amounts of water ice that might be present on the surface of 2007 JJ_{43}. This model allows us to constrain the reflectance spectra and the albedo of a medium using the physical properties of the different chemical components. The albedo (Alb) is approximated using Eq. (44) of Hapke (1981), which is a function of the bihemispherical reflectance for isotropic scatterers, r_0 and the average single-scattering albedo, w,

$$\mathrm{Alb} = r_0(0.5 + r_0/6) + (w/8)((1 + B_0)P(0) - 1) \quad (1)$$

where w depends on the optical constants and the size of the particles and is computed for a multicomponent surface (assumed to be intimately and/or geographically mixed, see Poulet et al. 2002). Here, B_0 is the ratio of the near-surface contribution to the total particle scattering at zero phase angle, and P is the phase function. B_0 is assumed to be close to 0.67 for icy objects (Verbiscer & Helfenstein 1998), and we used a Henyey-Greenstein function (Greenstein & Henyey 1941) for the phase function.

Because TNOs are generally observed at small phase angles, a good approximation is to set the angle to zero. We used the method described in Merlin et al. (2010), neglecting the surface roughness and the interference phenomenon known as coherent backscatter.

We degraded the spectral resolution of 200 to increase the S/N while keeping an acceptable resolution to identify possible absorption features.

We used the quadratic sum of the standard deviation of the data, ($\sqrt{\sigma^2 + \sigma^2_{\mathrm{pix}}}$), where σ is the standard deviation of the data

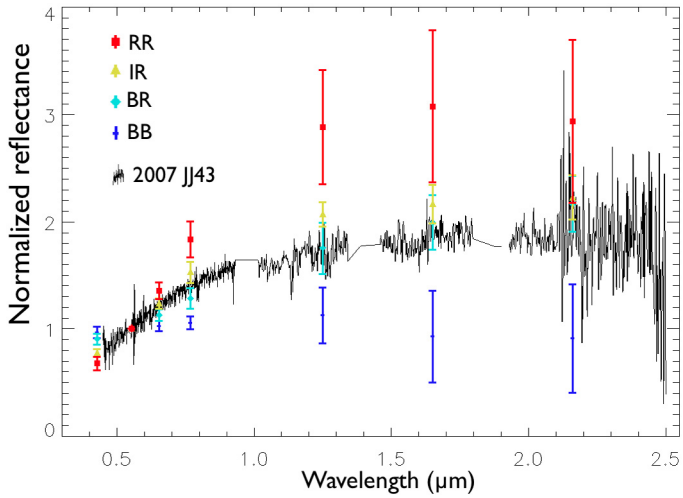

Fig. 4. Comparison of (278361) 2007 JJ_{43} spectra (black) with the values from Perna et al. (2010) with RR (red), IR (yellow), BR (green) and BB (blue). The spectrum and all photometric data were normalized to unity at 0.554 μm.

and σ_{pix} the standard deviation linked to the averaged pixels obtained to achieve the spectral resolution of 200.

4.2. Results for intimate mixtures

We used an intimate mixture of materials, meaning that a photon interacts with grains of more than one composition before being reflected off the surface. Surfaces are likely, however, to have some combination of horizontally separated patches, or vertical layers, and intimate mixtures of grains. We used optical constants of H_2O ice in its crystalline state (at 40 K from Grundy & Schmitt 1998), amorphous carbon (Zubko et al. 1996; in very small quantities), and Titan and Triton tholins (Khare et al. 1984, 1993). Triton tholin and Titan tholin are nitrogen-rich organic substances produced by the irradiation of gaseous mixtures of nitrogen and methane such as those found in the atmospheres of Triton and Titan. We recall that the atmosphere of Triton is to 99.9% composed of nitrogen and to 0.1% of methane, whereas that of Titan consists of 98.4% of nitrogen and 1.6% of methane and trace amounts of other gases). These atmospherically derived substances are distinct from ice tholin, which is formed by irradiation of clathrates of water and organic compounds such as methane or ethane. Carbon and tholins are used as representative material to aid fitting the low albedo and red slope of TNO spectra since optical constants are available for these materials. However, it must be noted that since they do not have any distinctive absorption band, their presence on these surfaces is not guaranteed. They could be replaced by different dark or red materials, such as other organics. In our model we also included kerogen, which is a mixture of organic chemical compounds that allows reproducing the slope of the visible spectrum while keeping the flatness in the near-infrared. We thus tested several models iterating with different albedos, quantities, and grain sizes with a minimization of the χ^2 between the model and the observed spectrum. The quality of the spectra does not allow distinguishing between crystalline and amorphous water ice. We use crystalline water ice as a reference here as it is detected for the largest observed TNO, and according to its diameter, it should be the case here. The models were mainly carried out to determine a limit for the presence of water ice. The noise of the spectra is relatively high and does not allow a more detailed study (χ^2 very small).

Four distinct models present the best fit (see Table 2):

- *Model 1*: this model considers a mixture of 6.4% of crystalline water ice with a grain size of 5 μm. The χ^2 obtained is equal to 0.014937.
- *Model 2*: this model is similar to model 1 except that the grain size of crystalline water ice is doubled (10 μm). A slightly lower concentration of water ice is obtained, 6.1%, and a slightly higher χ^2, 0.014972.
- *Model 3*: in this model, the grain size of water ice is still higher, 50 μm, but with a significant decline in its relative abundance (4.0%). The obtained χ^2 is still higher, 0.015202.
- *Model 4*: the last model has almost no water ice (relative abundance around 10^{-4}%). However, with a χ^2 (0.016023) increasing by less than 8% compared to the previous models, we cannot conclude on the complete absence of water ice on the surface of 2007 JJ_{43}.

The spectrum obtained for each model is shown in Figs. 5 and 6. A few other models were also considered with larger grain sizes, 10 μm for all compounds (except kerogen) but the correlation with the observed data was poorer. Therefore, we believe that the grains of these other compounds are probably small (around 5 microns). According to the obtained χ^2, which is very small for all the four models discussed above, we can assume that crystalline water ice is present in the mixture (models 1, 2 and 3 versus model 4) and with small grain sizes (about 5 μm). However, since we did not detect the crystalline water ice features at 1.56, 1.65, and 2.0 μm in the spectra, probably due to the low signal-to-noise ratio of the data, we can only limit its presence to no more than about 6.5%. As has been predicted for an object of this size by the study of Schaller & Brown (2007) and with the model updated in Brown et al. (2012), 2007 JJ_{43} is too small and too warm to retain volatile ices such as methane, nitrogen or carbon monoxide. The absence of icy elements observed on this object therefore perfectly agrees with this study. If we compare the characteristics obtained (absolute magnitude around 3.5 and water ice spectral fraction limited to 6.5%), the results are perfectly consistent with the trend observed for the large $H < 4$ trans-Neptunian objects (Brown et al. 2012, Fig. 2).

5. Conclusion

With the X-Shooter instrument based on the Very Large Telescope, we observed the trans-Neptunian object (278361) 2007 JJ_{43}, which is a good candidate to be a dwarf planet. The obtained spectrum simultaneously covers the ultraviolet, visible, near-infrared and extends from 0.3 up to 2.4 μm. The main results obtained can be resumed as follows.

- The spectrum of 2007 JJ_{43} is featureless and presents some reddening of the surface.
- The object can be taxonomically classified as BR (blue-red).
- No absorption band of icy elements was detected in the spectra, which agrees with the model described by Schaller & Brown 2007 (updated in Brown et al. 2012), which predicts that objects with sizes similar to that of 2007 JJ_{43} are too small and too warm to retain volatile ices such as methane, nitrogen, or carbon monoxide.
- With its absolute magnitude around 3.5 and its water ice spectral fraction limited to 6.5%, 2007 JJ_{43} is consistent with the trend observed for the large $H < 4$ trans-Neptunian objects (Brown et al. 2012).

Table 2. Intimate mixtures obtained with the four models.

Components	Kerogen	H_2O Cr.	Triton tholin	Titan tholin	Am. carbon
Model 1	χ^2 = 0.014937				
Mixtures %	43.8	6.4	38.0	11.8	<0.1
Grain size (μm)	100	5	5	5	5
Model 2	χ^2 = 0.014972				
Mixtures %	44.7	6.1	37.6	11.7	<0.1
Grain size (μm)	100	10	5	5	5
Model 3	χ^2 = 0.015202				
Mixtures %	49.8	4.0	35.4	10.9	<0.1
Grain size (μm)	100	50	5	5	5
Model 4	χ^2 = 0.016023				
Mixtures %	63.9	0.0	27.3	8.9	<0.1
Grain size (μm)	100	100	5	5	7

Notes. Am. = amorphous; Cr. = crystalline.

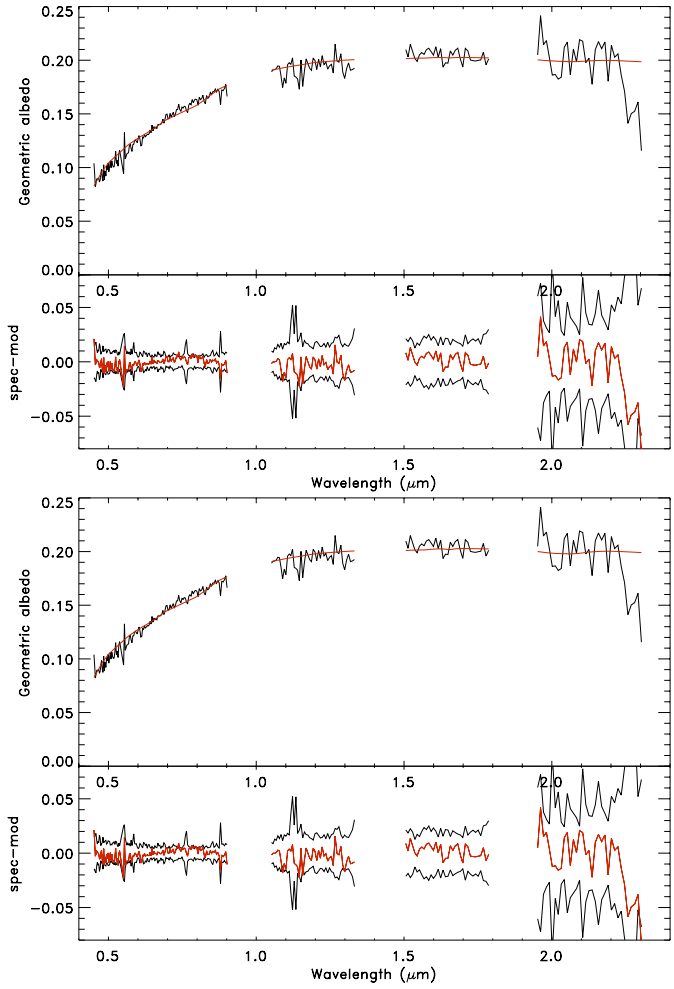

Fig. 5. Model 1 (*top*) and model 2 (*bottom*) considering the presence of crystalline H_2O with grain sizes of 5 and 10 μm, respectively (see Table 2 for details). In the *upper part* of each graphic, is plotted the observed spectrum (black) and the corresponding model (red), all normalized to 0.020 at 1.75 microns. In the *bottom part* is given the associated spectrum-model (red) and the noise (black) corresponding to the quadratic sum of the standard deviation of the data.

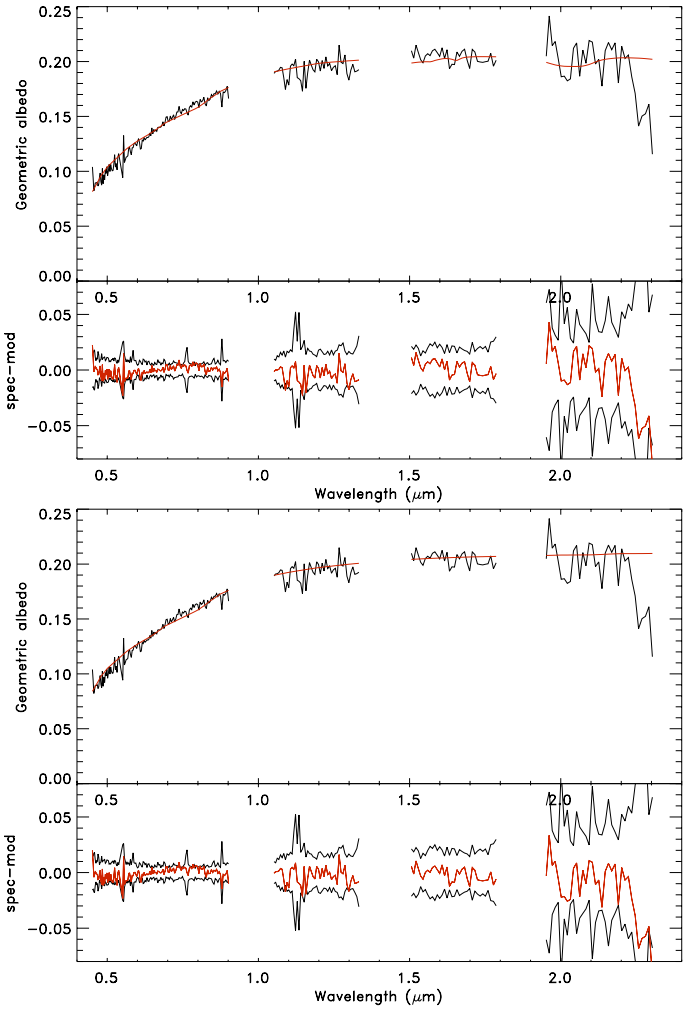

Fig. 6. Same as Fig. 5 but for Model 3 (*top*) and 4 (*bottom*), see Table 2 for details.

– We modeled intimate mixtures including various compounds mainly to determine an upper limit of the water ice abundance. In view of the results on the χ^2 (which are very small), it appears that the spectral noise is relatively high and does not allow a detailed study of the water ice properties. The obtained results indicate that a small amount of crystalline water ice (around 6% with a grain size of 5 μm) could be present on the observed surface. However, the absence of water ice, although less probable, cannot be ruled out.

– The observation of different regions of 2007 JJ_{43} show no significant differences suggesting an homogeneous surface or, at least that the observed surface is homogeneous, which is about one-third of the entire surface.
– We do not see much ice on spectra. This might be due to the low S/N, and feature absorption could be masked by the noise. However, it might also be attributed to space weathering, which is a combination of multiple ion sources contributing to the total energetic ion environment in the outer solar system from solar energetic particles, to anomalous cosmic rays, and Galactic cosmic rays.

References

Alvarez-Candal, A., Barucci, M. A., Merlin, F., Guilbert, A., & de Bergh, C. 2007, A&A, 475, 369
Barucci, M. A., Belskaya, I. N., Fulchignoni, M., & Birlan, M. 2005, AJ, 130, 1291
Benecchi, S. D., & Sheppard, S. S. 2013, AJ, 145, 124
Brown, M. E., Schaller, E. L., & Fraser, W. C. 2012, AJ, 143, 146
Greenstein, J. L., & Henyey, L. G. 1941, ApJ, 93, 327
Grundy, W. M., & Schmitt, B. 1998, J. Geophys. Res., 103, 25809
Hapke, B. 1981, J. Geophys. Res., 86, 3039
Hapke, B. 1993, Theory of reflectance and emittance spectroscopy (Cambridge University Press)
Khare, B. N., Sagan, C., Arakawa, E. T., et al. 1984, Icarus, 60, 127
Khare, B. N., Thompson, W. R., Cheng, L., et al. 1993, Icarus, 103, 290
Merlin, F., Barucci, M. A., de Bergh, C., et al. 2010, Icarus, 208, 945
Perna, D., Barucci, M. A., Fornasier, S., et al. 2010, A&A, 510, A53
Poulet, F., Cuzzi, J. N., Cruikshank, D. P., Roush, T., & Dalle Ore, C. M. 2002, Icarus, 160, 313
Schaller, E. L., & Brown, M. E. 2007, ApJ, 659, L61
Schwamb, M. E., Brown, M. E., Rabinowitz, D., & Marsden, B. G. 2007, Minor Planet Electronic Circulars, 14
Sheppard, S. S., Udalski, A., Trujillo, C., et al. 2011, AJ, 142, 98
Verbiscer, A., & Helfenstein, P. 1998, in Solar System Ices, eds. B. Schmitt, C. de Bergh, & M. Festou, Astrophys. Space Sci. Lib., 227, 157
Zubko, V. G., Mennella, V., Colangeli, L., & Bussoletti, E. 1996, MNRAS, 282, 1321